Evidence for Merger-driven Growth in Luminous, High-z, Obscured AGNs in the CANDELS/COSMOS Field

J. L. Donley[1], J. Kartaltepe[2], D. Kocevski[3], M. Salvato[4], P. Santini[5], H. Suh[6], F. Civano[7], A. M. Koekemoer[8],
J. Trump[9], M. Brusa[10], C. Cardamone[11], A. Castro[12,13], M. Cisternas[14], C. Conselice[15], D. Croton[16],
N. Hathi[17,8], C. Liu[18,19,20], R. A. Lucas[8], P. Nair[21], D. Rosario[4], D. Sanders[22], B. Simmons[23,31], C. Villforth[24,25],
D. M. Alexander[26], E. F. Bell[27], S. M. Faber[28], N. A. Grogin[8], J. Lotz[8], D. H. McIntosh[29], and T. Nagao[30]

[1] Los Alamos National Laboratory, P.O. Box 1663, Los Alamos, NM 87545, USA; jdonley@lanl.gov
[2] Rochester Institute of Technology, Rochester, NY, USA
[3] Colby College, Waterville, ME 04901, USA
[4] Max Planck Institut für extraterrestrische Physik, Giessenbachstrasse 1, D-85748 Garching bei München, Germany
[5] INAF-Osservatorio Astronomico di Roma, via di Frascati 33, I-00040, Monte Porzio Catone, Roma, Italy
[6] Subaru Telescope, National Astronomical Observatory of Japan, 650 A'ohoku place, Hilo, HI, 96720, USA
[7] Harvard-Smithsonian Center for Astrophysics, 60 Garden Street, Cambridge, MA 02138, USA
[8] Space Telescope Science Institute, 3700 San Martin Drive, Baltimore, MD 21218, USA
[9] University of Connecticut, 2152 Hillside Road, U-3046, Storrs, CT 06269, USA
[10] INAF-Osservatorio Astronomico di Bologna, via Ranzani 1, I-40127, Bologna, Italy
[11] Department of Math & Science, Wheelock College, 200 Riverway, Boston, MA 02215, USA
[12] Universidad Nacional Autónoma de México (UNAM), Instituto de Astronomía, Observatorio Astronómico Nacional. A.P. 877, 22800 Ensenada, BC, México
[13] Universidad Autónoma de Ciudad Juárez, Instituto de Ingeniería y Tecnología. 1210 Plutarco Elias Calles,32310 Cd. Juarez, CH, México
[14] Instituto de Astrofisica de Canarias, E-38205 La Laguna, Tenerife, Spain
[15] School of Physics & Astronomy, University of Nottingham, Nottingham, NG7 2RD, UK
[16] Centre for Astrophysics & Supercomputing, Swinburne University of Technology, P.O. Box 218, Hawthorn, Victoria 3122, Australia
[17] Aix Marseille Université, CNRS, LAM (Laboratoire d'Astrophysique de Marseille) UMR 7326, F-13388, Marseille, France
[18] Astrophysical Observatory, Department of Engineering Science and Physics, City University of New York,
College of Staten Island, 2800 Victory Boulevard, Staten Island, NY 10314, USA
[19] Department of Astrophysics and Hayden Planetarium, American Museum of Natural History, New York, NY 10024, USA
[20] Physics Program, The Graduate Center, CUNY, New York, NY 10016, USA
[21] Department of Physics and Astronomy, University of Alabama, Box 870324, Tuscaloosa, AL 35487-0324, USA
[22] Institute for Astronomy, University of Hawaii, 2680 Woodlawn Drive, Honolulu, HI 96822, USA
[23] Center for Astrophysics and Space Sciences, University of California, San Diego, La Jolla, CA 92093, USA
[24] University of Bath, Department of Physics, Claverton Down, Bath, BA2 7AY, UK
[25] Scottish University Physics Alliance (SUPA), University of St. Andrews, North Haugh, KY16 9SS, St. Andrews, UK
[26] Centre for Extragalactic Astronomy, Department of Physics, Durham University, South Road, Durham DH1 3LE, UK
[27] Department of Astronomy, University of Michigan, Ann Arbor, MI 48109, USA
[28] Department of Astronomy and Astrophysics, University of California Observatories/Lick Observatory, University of California, Santa Cruz, CA 95064, USA
[29] Department of Physics and Astronomy, University of Missouri-Kansas City, Kansas City, MO 64110, USA
[30] Research Center for Space and Cosmic Evolution, Ehime University, Bunkyo-cho 2-5, Matsuyama, Ehime 790-8577, Japan

Abstract

While major mergers have long been proposed as a driver of both active galactic nucleus (AGN) activity and the $M_{BH}-\sigma_{bulge}$ relation, studies of moderate to high-redshift Seyfert-luminosity AGN hosts have found little evidence for enhanced rates of interactions. However, both theory and observation suggest that while these AGNs may be fueled by stochastic accretion and secular processes, high-luminosity, high-redshift, and heavily obscured AGNs are the AGNs most likely to be merger-driven. To better sample this population of AGNs, we turn to infrared selection in the CANDELS/COSMOS field. Compared to their lower-luminosity and less obscured X-ray-only counterparts, IR-only AGNs (luminous, heavily obscured AGNs) are more likely to be classified as either irregular ($50^{+12}_{-12}\%$ versus $9^{+5}_{-2}\%$) or asymmetric ($69^{+9}_{-13}\%$ versus $17^{+6}_{-4}\%$) and are less likely to have a spheroidal component ($31^{+13}_{-9}\%$ versus $77^{+4}_{-6}\%$). Furthermore, IR-only AGNs are also significantly more likely than X-ray-only AGNs ($75^{+8}_{-13}\%$ versus $31^{+6}_{-6}\%$) to be classified either as interacting or merging in a way that significantly disturbs the host galaxy or as disturbed, though not clearly interacting or merging, which potentially represents the late stages of a major merger. This suggests that while major mergers may not contribute significantly to the fueling of Seyfert-luminosity AGNs, interactions appear to play a more dominant role in the triggering and fueling of high-luminosity heavily obscured AGNs.

Key words: galaxies: active – infrared: galaxies – X-rays: galaxies

1. Introduction

The origin of the evolutionary connection between supermassive black holes (SMBHs) and their host galaxies, as evidenced by the $M_{BH}-\sigma_{bulge}$ relation (Magorrian et al. 1998;

Gebhardt et al. 2000), remains one of the major open questions in extragalactic astronomy. For the past decade, theorists have invoked major mergers between gas-rich galaxies to explain not only this correlation, but also the strikingly similar cosmic evolution of active galactic nuclei (AGNs) and star formation activity (e.g., Hopkins et al. 2008).

---

[31] Einstein Fellow.

Not only are major mergers required to reproduce the properties of classical bulges in simulations of galaxy formation, but when coupled with feedback, mergers can reproduce many of the global properties of both the AGNs and galaxy populations, including the $M_{BH}-\sigma_{bulge}$ relation (Di Matteo et al. 2005; Hopkins et al. 2006, 2008; Robertson et al. 2006). Furthermore, the best examples of ongoing mergers in the local universe, ultraluminous infrared galaxies (ULIRGS), have long been known to be active sites of both intense star formation and AGN activity. This observation led to a proposed co-evolutionary scenario in which major mergers drive the growth of bulges via nuclear star formation and violent relaxation, and provide fuel to a rapidly accreting AGN via merger-induced gravitational torques (Sanders et al. 1988; Hopkins et al. 2008).

At first glance, studies of local ($z < 0.45$) QSOs appear to support this scenario, with 25%–100% showing evidence for ongoing mergers or tidal debris (Bahcall et al. 1997; Canalizo & Stockton 2001; Zakamska et al. 2006; Bennert et al. 2008; Greene et al. 2009; Veilleux et al. 2009a). While these small targeted studies indicate that local QSOs are commonly associated with mergers, the few studies that compare their morphologies to inactive control samples fail to find evidence for enhanced morphological disturbances (Dunlop et al. 2003; Reichard et al. 2009). QSOs, however, are rare in the local universe, and may not be triggered by the same mechanisms responsible for driving their high-redshift counterparts onto the $M_{BH}-\sigma_{bulge}$ relation, which was largely in place by $z \sim 1$ (e.g., Cisternas et al. 2011a). To determine the prevalence of mergers among high-redshift AGNs, we have therefore turned to the cosmological deep fields.

Studies of AGN hosts in the GEMS, GOODS, AEGIS, and COSMOS fields have predominantly targeted X-ray selected AGNs at $0.2 < z < 1.3$ (Sánchez et al. 2004; Grogin et al. 2005; Pierce et al. 2007; Gabor et al. 2009; Cisternas et al. 2011b; Simmons et al. 2012; Villforth et al. 2014; Rosario et al. 2015; Bruce et al. 2016). While a small fraction of these AGN hosts show strong distortions, the rate of morphological disturbances is similar to that of inactive galaxy control samples, suggesting that mergers do not play a dominant role in AGN fueling, at least out to $z \sim 1$. That said, there is evidence for a factor of $\sim$2.5 enhancement of Seyfert-level AGN activity in close pairs (Ellison et al. 2011; Silverman et al. 2011) and evidence that minor mergers may play a role in the fueling of moderate-luminosity AGNs (Altamirano-Dévora et al. 2016). Furthermore, Koss et al. (2010) find both an increased pair and merger fraction in local hard X-ray AGN samples.

To extend this analysis to the peak of AGN activity at $z \sim 2$, we turn to the near-IR *HST*/WFC3 CANDELS survey, which probes light redward of the 4000 Å break and thus traces emission from the stars responsible for the bulk of the stellar mass. Initial studies of the hosts of $z \sim 2$ X-ray AGNs in the GOODS-S region of CANDELS, however, likewise find morphologies that are indistinguishable from those of normal star-forming galaxies (Schawinski et al. 2011; Kocevski et al. 2012; Simmons et al. 2012). Furthermore, the high incidence of disk galaxies, which should be destroyed by major mergers, suggests that a time delay between merger activity and the AGN phase cannot account for the lack of merger signatures.

While these observations appear to call into question the role of major mergers in AGN/galaxy coevolution, most X-ray AGN populations studied thus far are dominated by low-luminosity Seyfert galaxies ($\log L_{0.5-10\,keV}$ (erg s^{-1}) < 44), which may be experiencing a different mode of SMBH and galaxy growth than their high-luminosity counterparts. For instance, while cosmological simulations require mergers to reproduce the properties of luminous QSOs, stochastic accretion and secular processes can account for the lower levels of nuclear activity in Seyfert galaxies (Hopkins & Hernquist 2006; Hasinger 2008; Hopkins et al. 2008, 2014; Hopkins & Hernquist 2009). This hypothesis appears to be backed by a growing number of studies that find a larger merger-driven and disturbed fraction among high-luminosity AGNs across a range of redshifts (Guyon et al. 2006; Urrutia et al. 2008; Kartaltepe et al. 2010; Koss et al. 2012; Treister et al. 2012; Glikman et al. 2015; Ellison et al. 2016; Fan et al. 2016), though there are exceptions (Villforth et al. 2014; Mechtley et al. 2016; Villforth et al. 2017). A similar trend has been observed in both the local and high-z infrared and SMG galaxy populations, where late-stage major mergers are responsible for fueling nearly all of the most luminous galaxies (Engel et al. 2010; Ivison et al. 2012; Larson et al. 2016).

If the merger-driven evolutionary scenarios summarized in Hopkins et al. (2008) and Alexander & Hickox (2012) are correct, the early phases of a major merger should be dominated by luminous, yet heavily obscured, AGN activity. As the SMBH grows, AGN feedback then serves to remove the dust and gas and the AGN becomes dust reddened and eventually unobscured, but only after the fading merger features become difficult to identify, particularly in the distant universe. To test the major merger scenario for the coevolution of SMBHs and their hosts, studies should therefore target not only luminous AGNs, but heavily obscured luminous AGNs. While doing so can be difficult using soft X-ray and optical emission alone, the same dust and gas that serves to obscure the AGNs' signatures also acts like a natural coronagraph, blocking the intense UV-optical radiation from the AGN itself and permitting a study of the underlying host galaxy emission.

A number of studies have begun to target obscured AGNs at both low and high luminosity, and most (Schawinski et al. 2012 is an exception) have indeed found a higher rate of disturbances among more heavily obscured samples (Koss et al. 2010; Urrutia et al. 2012; Satyapal et al. 2014; Kocevski et al. 2015; Ellison et al. 2016; Fan et al. 2016; Shangguan et al. 2016; Weston et al. 2017) or evidence that extinction peaks during the intermediates stages of merger evolution (Veilleux et al. 2009b), albeit with a strong chaotic component. This suggests that AGN unification is not due solely to orientation (Cattaneo et al. 2005; Kocevski et al. 2015).

High-luminosity, high-redshift, and heavily obscured AGNs therefore comprise the population of AGNs most likely to experience merger-driven SMBH and galaxy coevolution. Fortunately, these AGNs can effectively be targeted using their mid-IR colors. For an AGN to be identified via its MIR colors, its hot dust emission must overpower the underlying stellar emission from the host galaxy (e.g., Donley et al. 2008, 2012). MIR selection therefore identifies the most luminous, and thus the highest-redshift ($z \sim 2$) AGNs in the limited volumes probed by deep survey fields, recovering few Seyfert galaxies but >75% of X-ray AGNs with QSO luminosities (Donley et al. 2012). Furthermore, because NIR-MIR emission is largely insensitive to intervening obscuration, the unique MIR power-law signature of luminous AGNs is observable in both unobscured and heavily obscured AGNs. MIR selection

therefore provides a way to recover highly complete samples of luminous, high-z, and heavily obscured AGNs, exactly those AGNs whose evolution is expected to be dominated by major mergers (Alonso-Herrero et al. 2006; Donley et al. 2007, 2010, 2012).

In the work that follows, we directly compare for the first time the morphologies of X-ray and infrared-selected AGNs. If mergers do indeed play a dominant role in the triggering of luminous, high-z, obscured AGNs, we should see an excess of merger signatures in our sample of high-luminosity, heavily obscured IR-only AGNs when compared to the lower-luminosity, less heavily obscured X-ray-only population.

This paper is organized as follows. In Section 2, we discuss the relevant data in the CANDELS/COSMOS field and describe our selection of the infrared and X-ray AGN samples. The sample properties (reliability, redshifts, luminosities, and stellar masses) are given in Section 3. In Section 4, we present the visual classification scheme as well as the resulting morphologies for the infrared and X-ray AGN samples. The conclusions are given in Section 5. Throughout the paper, we assume the following cosmology: $(\Omega_{\mathrm{m}}, \Omega_{\Lambda}, H_0) = (0.27, 0.73, 70.5 \ \mathrm{km \ s^{-1} \ Mpc^{-1}})$.

2. Data and Sample Selection

We selected the AGN for this study from the $\sim$200 sq. arcmin CANDELS/COSMOS field. The CANDELS survey imaged the central region of the COSMOS field in both the WFC3 F125W (J-band) and F160W (H-band) filters to 5σ limiting AB magnitudes of 27.72 and 27.56, respectively (see Koekemoer et al. 2011 and Nayyeri et al. 2017 for details on the CANDELS *HST* data products). This high-resolution NIR imaging data provides a crucial look at the rest-frame optical emission from moderate to high-redshift galaxies and AGNs.

The COSMOS survey provides ample multiwavelength data over the field, including the X-ray (*XMM* and *Chandra*) and MIR (*Spitzer* IRAC) coverage most relevant to this work. Shallow ($\sim$40 ks) *XMM* data extends over the full COSMOS field (Hasinger et al. 2007; Cappelluti et al. 2009; Brusa et al. 2010), whereas the deeper *Chandra* coverage used here is limited to the central 0.9 deg², but fully covers the CANDELS/COSMOS field with an average exposure time of $\sim$170 ks. (Deeper *Chandra* data now exist in the outer regions of the COSMOS field—Civano et al. 2016—but do not overlap the CANDELS field.)

The primary *Spitzer* IRAC data used for this study (Sanders et al. 2007) cover the full COSMOS field to 1200 s depth, or 5σ sensitivities of 0.9, 1.7. 11.3, and 14.6 μJy in the 3.6, 4.5, 5.8, and 8.0 μm bands, respectively. We exclude from our study all IRAC sources that lie within the masked regions of bright ($K < 14$) 2MASS sources, but include sources with flags indicating nearby neighbors or deblending. Of the $\sim$1000 IRAC sources that fall within the CANDELS/COSMOS field and that are brighter than the 5σ sensitivities in each of the IRAC bands, 9% have either bad pixels or neighbors bright and close enough to significantly bias the photometry and 11% were originally blended with another object (note that these are not mutually exclusive). Of the 43 infrared-selected AGNs (IRAGNs) we will select using this data, 5 (12%) are flagged as having nearby neighbors or were blended with another object, but a careful inspection of each source indicates that the IRAGN selection is robust to these issues. Furthermore, our comparison below with the COSMOS15 IRAC photometry

(see Section 3.1) provides an additional check on the IRAGN selection reliability.

2.1. IRAGN

IRAGNs were selected directly from the Sanders et al. (2007) IRAC catalog using the criteria outlined in Donley et al. (2012):

$$x = \log_{10}\left(\frac{f_{5.8 \ \mu\mathrm{m}}}{f_{3.6 \ \mu\mathrm{m}}}\right), \quad y = \log_{10}\left(\frac{f_{8.0 \ \mu\mathrm{m}}}{f_{4.5 \ \mu\mathrm{m}}}\right) \quad (1)$$

$$x \geqslant 0.08 \wedge y \geqslant 0.15$$
$$\wedge y \geqslant (1.21 \times x) - 0.27 \wedge y \leqslant (1.21 \times x) + 0.27$$
$$\wedge f_{4.5 \ \mu\mathrm{m}} > f_{3.6 \ \mu\mathrm{m}} \wedge f_{5.8 \ \mu\mathrm{m}} > f_{4.5 \ \mu\mathrm{m}} \wedge f_{8.0 \ \mu\mathrm{m}} > f_{5.8 \ \mu\mathrm{m}}.$$
$$(2)$$

As in Donley et al. (2012), we require that IRAGNs have fluxes that exceed the 5σ sensitivities in each of the IRAC bands (see above). We experimented with loosening this criterion, but the vast majority of additional sources we select were not clearly visible in either of the 5.8 or 8.0 μm bands. In total, we identify 43 IRAGNs across the CANDELS/COSMOS field. We cross-check the IRAGN selected using the Sanders et al. (2007) catalog against those selected using the Laigle et al. (2016) COSMOS15 catalog in Section 3.1 below.

After selecting the IRAGN, we located the nearest CANDELS H-band source using a search radius of 2″. By directly matching the IRAC and H-band catalogs, we avoided imposing a criterion that there be a visible (I-band) counterpart. In most cases, this made no practical difference, but for three IRAGNs, the nearest H-band source has no corresponding optical counterpart in the Subaru I-band catalog of Ilbert et al. (2009). In contrast, all IRAGNs had an H-band counterpart, with median and maximum offsets of 0″12 and 0″56, respectively.

2.2. X-Ray AGNs

X-ray AGNs were selected from the *Chandra* catalog of Civano et al. (2012).[32] We match the H-band catalog directly to the X-ray positions. Of the 99 *Chandra* sources, all but 3 have a clear H-band counterpart within the 2″ radius. One of these sources was later removed from our sample because it falls below our X-ray luminosity cut. For the remaining two sources, we searched for an H-band counterpart using the optical counterpart position given in Civano et al. (2012). One has an H-band counterpart only 0″11 from the optical position, the other has no H-band counterpart, and is therefore excluded from our study.

Starting from the H-band, as opposed to the optical I-band, allowed us to identify clear counterparts for four *Chandra* sources that have no Subaru optical counterparts (Ilbert et al. 2009) in Civano et al. (2012). For the remaining sources, the optical counterpart nearest our H-band counterpart matches the optical counterpart identified by Civano et al. (2012).

---

[32] 60 sources in our sample have *XMM* counterparts from Brusa et al. (2010). Of these, all but six have *Chandra* counterparts. We carefully examined these six sources, and found that only one, also an IRAGN, had a visible excess of *Chandra* counts near the *XMM* source position. While we therefore consider this source to be X-ray detected, we exclude the remaining *XMM*-only sources from our sample as all are detected in only one of the *XMM* bands (full/hard/ soft) to $\leqslant 6\sigma$. This choice has no effect on the final conclusions of this work.

3. Sample Properties

Our full sample of X-ray and infrared-selected AGNs consists of 43 IRAGN, 16 of which have no X-ray counterparts, and 72 *Chandra* or XMM-selected AGNs that are *not* IRAGNs (or that fall below the IRAC flux cuts in one or more of the IRAC bands). IRAGN selection predominantly identifies the most intrinsically luminous AGNs (see Section 3.4), and the IRAGNs lacking X-ray counterparts are likely to be luminous but heavily obscured (Donley et al. 2012). In contrast, the X-ray-only sample should predominantly lie at lower luminosities and/or redshifts and be dominated by sources with low to moderate obscurations. As such, it will serve as our control sample for comparison to the higher luminosity and higher-redshift IRAGNs.

3.1. IRAGN Selection Reliability

To check the reliability of the IRAGN selected using the Sanders et al. (2007) catalog, we turn to the COSMOS15 catalog (Laigle et al. 2016), a NIR-based catalog with PSF-matched photometry from the UV to the MIR. COSMOS15 takes advantage of the deeper data in IRAC channels 1 and 2 provided by the SEDS and SPLASH COSMOS surveys (see P. L. Capak et al. 2017, in preparation), but uses the same data presented in Sanders et al. (2007) for IRAC channels 3 and 4. However, for these two longer-wavelength channels, the error estimates from COSMOS15 are far more conservative than those given by Sanders et al. (2007), and the agreement between the catalogs begins to break down for sources with moderate Sanders et al. (2007) S/N but COSMOS15 S/N < 3 in one or more of the IRAC bands.

If we require that our IRAGNs be selected as such based on both the Sanders et al. (2007) and COSMOS15 catalogs, our sample of X-ray-detected IRAGNs drops by four from 27 to 23. The four sources that are lost all have COSMOS15 S/N > 3 in each of the IRAC bands, but the modest differences in photometry tend to place the Sanders et al. (2007)-selected IRAGNs just outside of the selection box.

Because X-ray undetected IRAGNs tend to be fainter than their X-ray-detected counterparts, the discrepancy between the catalogs at low COSMOS15 S/N has a far larger effect on our sample of X-ray undetected IRAGNs. Of the 16 Sanders et al. (2007)-selected IRAGNs without X-ray counterparts, only 7 would also be selected as IRAGNs using the COSMOS15 photometry (all 7 have COSMOS15 S/N > 3 in each IRAC band). We make the case below for keeping an additional two sources, bringing the number of X-ray undetected AGNs to nine, but the cross-check with COSMOS15 may remove as many as 7 of the 16 IRAGNs identified by Sanders et al. (2007).

Of these seven IRAGN not selected using COSMOS15, five have a COSMOS15 S/N $\lesssim$ 3 in IRAC channel 4 and largely discrepant channel 4 fluxes between the two catalogs, and two have S/N > 3 but were already marginal IRAGNs. Whether these sources are indeed IRAGNs or not therefore appears to be catalog-dependent, and we will consider both cases in the analysis below. As for the remaining two X-ray-undetected IRAGNs not identified by COSMOS15, one lacks a COSMOS15 counterpart altogether but has a high Sanders et al. (2007) S/N in all IRAC bands and the other is a single IRAC source whose flux appears to have been split between two optical/NIR counterparts in COSMOS15. Furthermore, for the
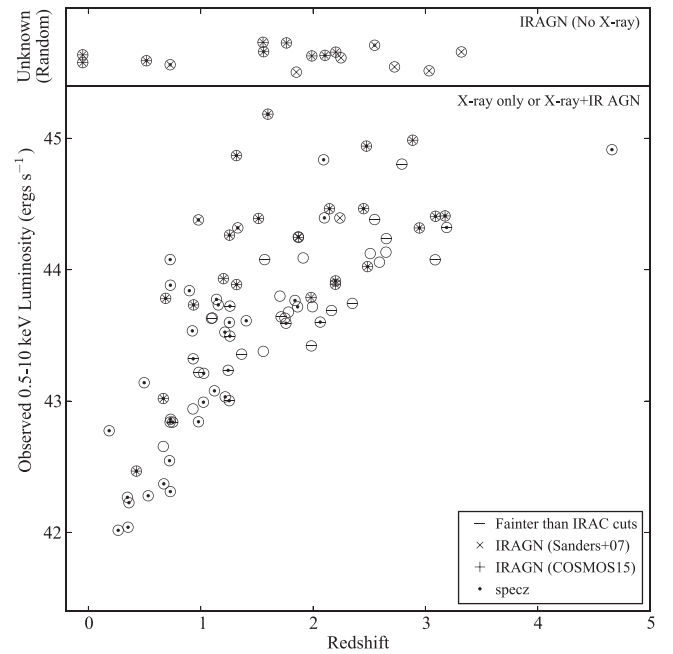

Figure 1. Observed $0.5-10$ keV X-ray luminosity vs. redshift for the IR and X-ray selected AGNs. IR-only AGNs are shown on the top, where their unknown "X-ray luminosity" has been randomized for plotting purposes and sources with unknown redshifts are assigned a value of -0.1. The vast majority of high-luminosity X-ray AGNs are also selected as IRAGNs, whereas most X-ray-only AGNs are Seyfert galaxies.

latter, only its slightly non-monotomic COSMOS15 IRAC fluxes cause it to not meet our strict IRAGN criteria: its COSMOS15 photometry places it inside the IRAGN selection box. We therefore keep both IRAGNs in our COSMOS15 sample, which can generally be viewed as a higher S/N subsample of the full Sanders et al. (2007)-selected IRAGN sample. The impact of this IRAC S/N cut on our results will be discussed below in Section 4.1.

3.2. Redshifts

Of the 115 AGNs in our full sample, 69 have spectroscopic redshifts from either public or internal COSMOS team data sets obtained using the following instruments or surveys: DEIMOS (Keck), FMOS (Subaru), FORS1 (VLT), FORS2 (VLT), FOCAS, *HST* Grism, IMACS (*Magellan*), LRIS (Keck), MOSFIRE (Keck), PRIMUS (*Magellan*/IMACS), SDSS, VIMOS (zCOSMOS), XSHOOTER (VLT), and 3DHST. The spectroscopic redshift fraction is $\sim$60% for both the IRAGNs and X-ray-only samples. For the remaining X-ray detected AGNs with optical counterparts, we adopt the AGN-specific photometric redshifts calculated by Salvato et al. (2011), and for the IRAGNs lacking X-ray counterparts, we calculate photometric redshifts using the methods outlined in Salvato et al. (2011) for consistency. Doing so gives redshift measurements or estimates for all but the three IRAGNs and four X-ray-only AGNs that lack clear optical counterparts. The median redshifts for the Sanders et al. (2007) and COSMOS15 IRAGN samples are $z = 1.93$ and $z = 1.87$, respectively, and that of the X-ray-only sample is $z = 1.22$.

3.3. Observed X-Ray Luminosities

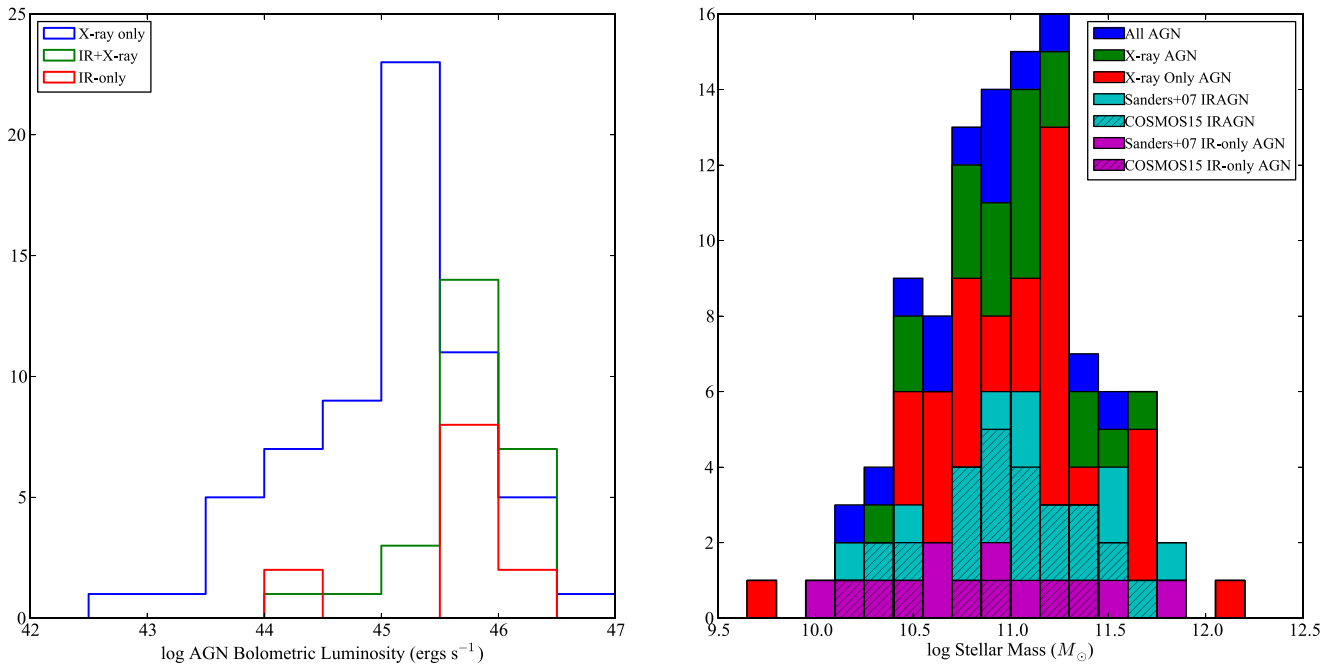We plot in Figure 1 the redshifts and observed 0.5–10 keV X-ray luminosities for our AGN samples. We have excluded

Figure 2. Left: AGN bolometric luminosity for the IR-only, IR+X-ray, and X-ray-only AGN populations. Bolometric luminosities were derived from SED fitting for sources with 24 μm counterparts, and from the X-ray luminosity for sources without 24 μm counterparts. IRAGN selection preferentially identifies the most intrinsically luminous AGNs. Right: stellar mass distribution for the various AGN subsamples, which are consistent with having been drawn from the same population.

from the X-ray-only sample four X-ray sources with luminosities lower than 10^{42} erg s^{-1}. We also identify in Figure 1 those AGNs that meet the IRAGN criteria.

As can be seen in Figure 1, 80% of the high luminosity ($L_x > 10^{44}$ erg s^{-1}) X-ray AGNs with good IRAC fluxes are also IRAGNs. In contrast, only 25% of the lower-luminosity ($L_x < 10^{44}$ erg s^{-1}) X-ray AGNs with good IRAC fluxes are IRAGNs, and 80% of these have X-ray luminosities greater than 5×10^{43} erg s^{-1}. As expected, the IRAGN selection effectively identifies the highest luminosity AGN, whereas the X-ray selection is sensitive to lower-luminosity Seyfert galaxies.

3.4. Bolometric Luminosities

Using the COSMOS15 catalog and the SED-fitting approach of Suh et al. (2017), which requires both a redshift and a 24 μm detection, we calculate the AGN bolometric luminosity for 76 of the 111 AGNs in our sample. The requirements listed above exclude four IR-only AGNs (one with no COSMOS15 counterpart, one with no redshift, and two that are blended with brighter nearby sources and so have no reported 24 μm fluxes), as well as 31 X-ray sources (2 with no COSMOS15 counterpart, 4 with no redshift, and 25 with no 24 μm counterpart).

For X-ray AGNs with redshifts, we can also estimate the AGN bolometric luminosity using the absorption-corrected rest-frame 0.5–10 keV X-ray luminosities from Marchesi et al. (2016a) and Marchesi et al. (2016b), where we give preference to the results from X-ray spectral fitting (Marchesi et al. 2016b) when they are available[33] (Note that for sources with only an upper limit on N_H, we apply no absorption correction, and for

sources with only a lower limit on N_H, we apply the correction associated with this lower limit.) Of the 94 *Chandra* sources in our sample, 62 have both an SED-derived bolometric luminosity as well as an X-ray luminosity. Comparing the AGN luminosities for this subsample gives an X-ray bolometric correction of $k_{bol} = 44$, in agreement with Hopkins et al. 2007 for an AGN sample with the median bolometric luminosity of our sample: 11.9 $L_\odot$. The scatter about the resulting L_{bol}(SED) versus L_{bol}(X-ray) relation has a standard deviation of $\sigma (\log L_{bol}) = 0.45$. Using this bolometric correction, we estimate the AGN bolometric luminosity for the remaining 26 X-ray sources in our sample with a redshift but no 24 μm counterpart. Combining these X-ray-derived AGN bolometric luminosities with the SED-derived AGN bolometric luminosities gives the distributions shown in Figure 2, where we give preference to the SED-derived L_{bol} when it is available.

As expected, and as was demonstrated using the X-ray luminosities in Figure 1 for AGNs with X-ray counterparts, IRAGN selection preferentially identifies the most intrinsically luminous AGNs. (The two IR-only AGNs with $\log L_{bol}$(erg s^{-1}) < 44.5 are the two IRAGNs in Figure 1 with $z < 1$.)

3.5. Stellar Masses

To ensure that our morphological analysis is not biased by the underlying stellar mass distribution of the various AGN samples, we also plot in Figure 2 the distribution of stellar masses calculated using the techniques described in Santini et al. (2012), which take into account both the stellar and AGN contributions to the SED. As can be seen, there is no systematic offset between the stellar masses of the X-ray and IR-selected samples. Instead, as confirmed by KS tests between the full AGN sample and various subsamples, as well as between the IR-only and X-ray-only subsamples (p-value = 0.46), the AGN subsamples are well-matched in stellar mass.

---

[33] We apply a correction factor to the X-ray luminosities from Marchesi et al. (2016a) to correct for a systematic offset between this catalog and Marchesi et al. (2016b) due to an inconsistency between the assumed spectral shapes (F. Civano 2017, private communication).
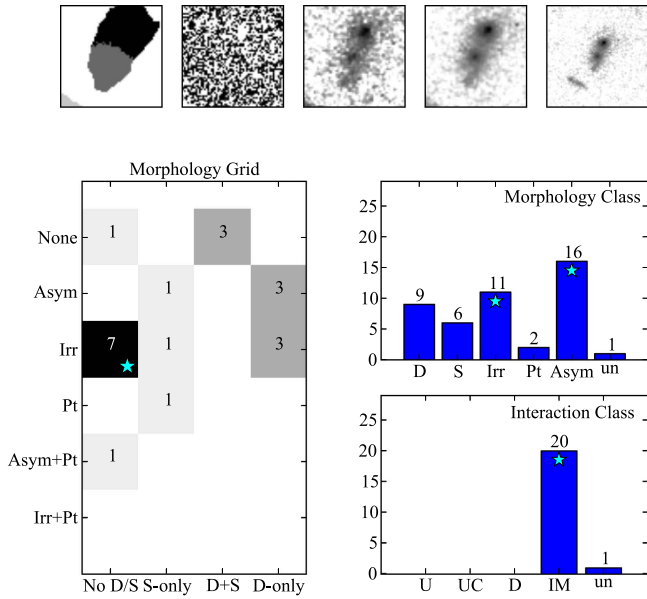
Figure 3. Morphology classification for one of the X-ray non-detected IRAGNs. From left to right, the thumbnails at the top show the segmentation map along with the ACS F814W I-band image, WFC3 F125W J-band image, and WFC3 F160W H-band images both at the nominal size and twice that to identify nearby companions. The morphology grid shows the combination of classes (Disk, Spheroid, Asymmetric, Irregular, Point Source) chosen by each of the 21 classifiers. The histograms then show the morphology and interaction classes described in Section 4 (recall that all sources identified as irregular are also considered to be asymmetric). The final consensus classifications (morphology = Irregular/Asymmetric, interaction = Interacting/Merging) are given by cyan stars.

4. Visual Morphologies

To determine the morphologies of our AGN sample, we utilized the CANDELS visual classification framework as described in Kartaltepe et al. (2015). For this study, the classification GUI displayed the Subaru V-band, *HST* ACS F814W (I-band), *HST* WFC3 F125W (J-band), and *HST* WFC3 F160W (H-band) images for each AGN. Twenty-one classifiers (all professional astronomers) then chose one or more of the following morphology classes for each AGN: disk, spheroid, peculiar/irregular, compact/point source, and unclassifiable. They then selected just one of the following interaction classes: merger, interaction within the segmentation map, interaction outside the segmentation map, non-interacting companion, and no interaction. Classifiers also had the option of selecting from a number of flags, including tidal arms, double nuclei, asymmetric, and point-source contamination. It is worth noting that while classifiers knew they were classifying a sample of AGNs, they did not know which AGNs were X-ray or IR-selected.

From these raw classifications, we created the following consensus classification categories for each source. For morphology, we added the asymmetric flag to our morphology classification (and flagged asymmetric in all cases where irregular had been chosen), resulting in the following non-mutually exclusive classes: disk, spheroid, irregular, point source (which also includes the point-source contamination flag), asymmetric, and unclassifiable. Following Kocevski et al. (2012), our consensus morphology class was then taken to be the combination of classes chosen by at least half (11+) of the classifiers. We show an example in Figure 3, where we plot the thumbnail images and individual

morphology classifications for one of the IRAGNs not detected in X-rays. In this particular case, the consensus morphology is Irregular+Asymmetric.

To determine the interaction class, we created the following five categories: undisturbed (no companion, interaction, merger, asymmetry, double nuclei, or tidal arms), undisturbed with a companion (companion, but no interaction, merger, asymmetry, double nuclei, or tidal arms), disturbed (no clear interaction or merger, but yes to asymmetry, double nuclei, or tidal arms), interaction or merger (either inside or outside the segmentation map), and unclassifiable. Our consensus interaction class was taken to be the most commonly selected of these five mutually exclusive classes. In the example shown in Figure 3, nearly all of the classifiers agree that this particular AGN is in an interacting or merging system.

For those sources classified as interacting or merging, we then separated them into two additional subclasses: interacting/merging and disturbed (interactions/mergers where the asymmetric, double nuclei, or tidal arm flags had been selected as well) and interacting/merging yet relatively undisturbed (interactions/mergers where none of the asymmetric, double nuclei, or tidal arm flags were selected). In general, the latter class tends to catch early and/or wide separation mergers as well as minor mergers.

We plot in Figure 4 the WFC3 F160W thumbnail images of our AGN sample, broken down by interaction type, and also identify those AGNs that are X-ray and/or infrared selected.

4.1. Morphology by AGN Type

We plot in Figure 5 two comparisons between the morphology and interaction classes for the X-ray and IR-selected AGN samples, where we separate the sample into IRAGN-only (no X-ray), X-ray+IRAGN, and X-ray only. The fractions for each category and subsample are given in Table 1. The figure on the left compares our full X-ray and Sanders et al. (2007)-selected IRAGN samples with one exception: we remove any AGN with a spectroscopic Type 1 identification to address the potential issue of rest-frame optical emission from the AGN masking the underlying morphology of the system. Removing the broad-line AGN (BLAGN) primarily impacts the unobscured, high-luminosity population that is both X-ray and IR-selected (15 AGNs are known BLAGNs, and 11 of these are also IRAGN). Of these 15 sources, 8 were classified as point sources by more than half of the classifiers, and 6 additional sources were classified as having a point source component by more than 20% of the classifiers. While it can occasionally be difficult for classifiers to distinguish between spheroids and point sources, the additional confirmation of a Type 1 spectrum indicates that we may not be seeing the underlying host galaxy emission in these systems. This restriction lowers the relative point-source fraction for the X-ray+IR AGN sample and subsequently raises the fractions for the remaining morphologies.

The figure on the right further restricts the IRAGN samples to those sources also selected using the COSMOS15 catalog (see Section 3.1). In this plot, we also remove any X-ray-only AGNs that fall below our flux cuts in one or more of the Sanders et al. (2007) IRAC bands or that have S/N < 3 in one or more of the COSMOS15 IRAC bands.

Because these X-ray AGNs are faint in the IR, we cannot determine whether or not they would meet the IRAGN criteria. This restriction impacts only the X-ray-only sample and results
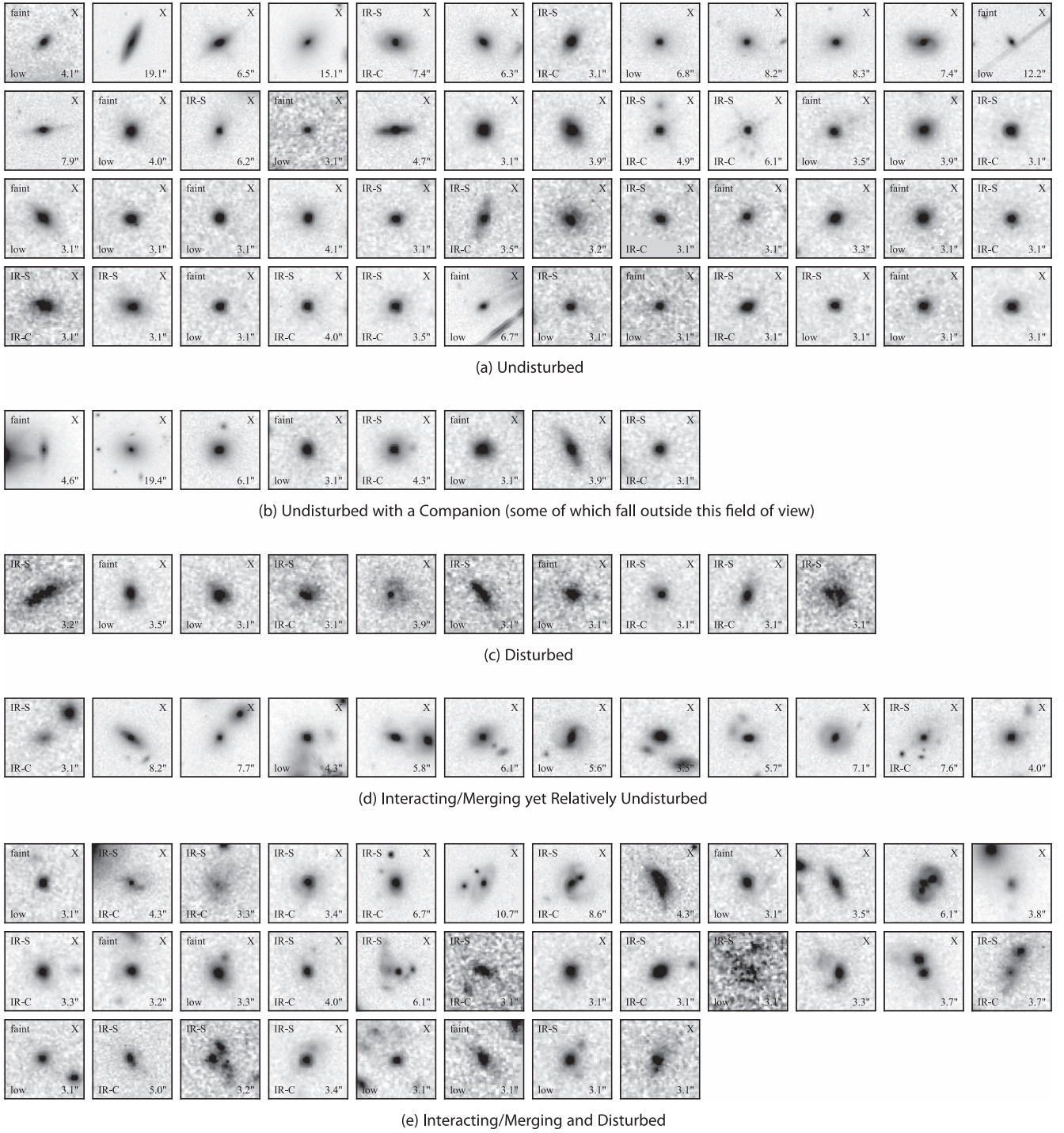
(a) Undisturbed

(b) Undisturbed with a Companion (some of which fall outside this field of view)

(c) Disturbed

(d) Interacting/Merging yet Relatively Undisturbed

(e) Interacting/Merging and Disturbed

Figure 4. WFC3 F160W thumbnail images for the X-ray and IR-selected AGN samples, broken down by the consensus interaction class. Sources detected in the X-ray have an "X" in the upper right corner. IRAGNs selected using Sanders et al. (2007) are indicated with an "IR-S" in the upper left, where "faint" means that the source falls below the IRAC detection limits in at least one band. IRAGNs also selected using COSMOS15 are indicated with an "IR-C" in the bottom left, where "low" means that the source has $S/N < 3$ in at least one band. The diameter of each image is given in the lower right. Each thumbnail is scaled to the size of the galaxy with a minimum size of $3\overset{''}{.}1$ (see Kartaltepe et al. 2015 for more details). It is worth noting that classifiers were shown thumbnails that match those shown here, as well as an H-band thumbnail twice as large to help identify potential companions.

in subtle changes to the morphology and interaction classes. In fact, we placed this restriction on the X-ray sources primarily to illustrate the fact that it has little impact on the results, aside from increasing the binomial confidence error bars calculated using the method of Cameron (2011).

As can be seen from Figure 5, the main conclusions of this study are insensitive to whether the IRAGNs are selected from

Sanders et al. (2007) or COSMOS15. There are of course subtle differences between the two samples, and the lower sample size for the COSMOS15 IRAGNs increases the error bars, but the trends discussed below hold regardless of the catalog we use to identify IRAGNs.

Focusing first on the morphological classes, we see that the IR-only AGNs, which tend to be heavily obscured, high-luminosity,
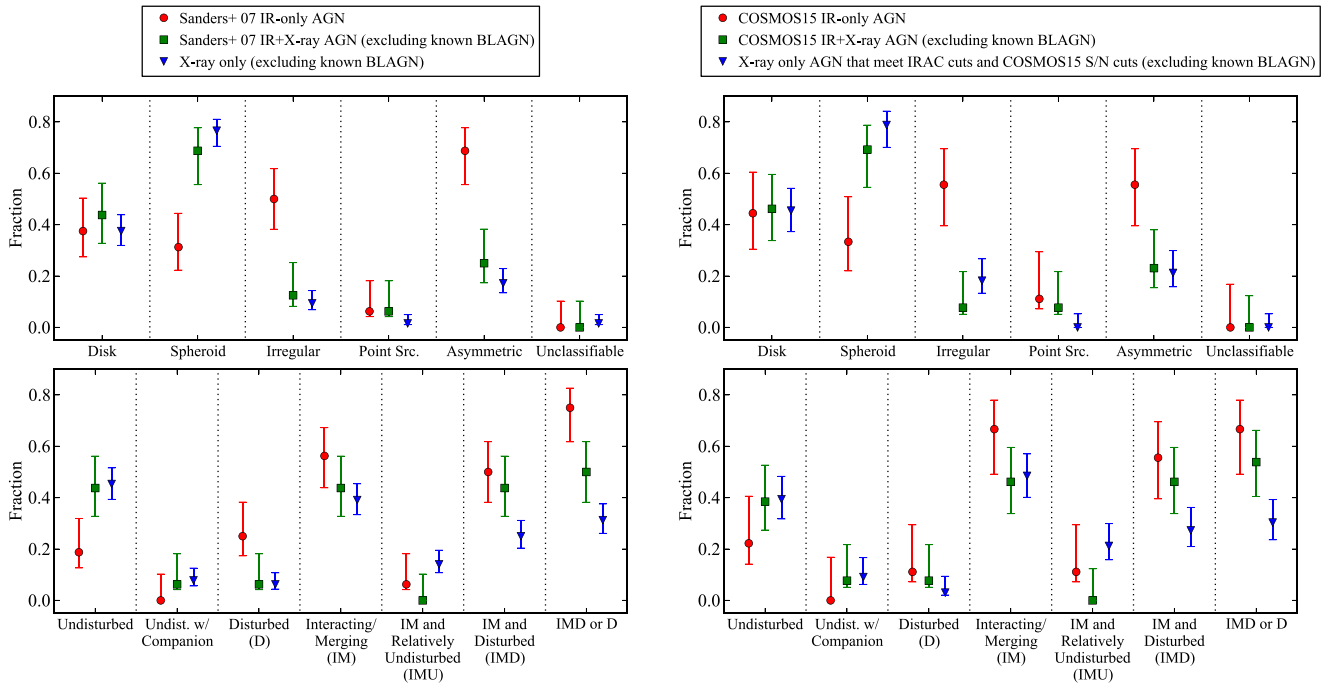
Figure 5. Comparison between the fraction of AGNs in the various morphology (disk, spheroid, irregular, point source, asymmetric, and unclassifiable) and interaction (undisturbed, undisturbed with a companion, disturbed, interacting/merging, interacting/merging+relatively undisturbed, and interacting/merging and disturbed) classes, broken down by the AGN sample (IR-only, IR+X-ray, X-ray-only). The plot on the left shows our full X-ray and Sanders et al. (2007)-selected IRAGN samples (with the exception of known BLAGNs), whereas the plot on the right further restricts the IRAGN sample to those sources also identified using the COSMOS15 catalog and removes any X-ray AGNs whose Sanders et al. (2007) IRAC fluxes or COSMOS15 S/N are too low to determine if they would meet the IRAGN selection criteria. Binomial confidence error bars are calculated using the method of Cameron (2011).

and high-redshift AGNs, are significantly more likely than X-ray-only AGNs to have been classified as irregular ($50^{+12}_{-12}\%$ versus $9^{+5}_{-2}\%$) or asymmetric ($69^{+9}_{-13}\%$ versus $17^{+6}_{-4}\%$), and are significantly less likely to have been classified as having a spheroidal component ($31^{+13}_{-9}\%$ versus $77^{+4}_{-6}\%$) (all at the $>3\sigma$ level). Their disk fraction is indistinguishable from the other samples. As for their interaction class, these luminous, heavily obscured AGN are less likely than X-ray-only AGN to be undisturbed ($19^{+13}_{-6}\%$ versus $45^{+6}_{-6}\%$) and are more likely to be both "disturbed" ($25^{+13}_{-8}\%$ versus $6^{+5}_{-2}\%$), and "interacting/merging and disturbed" ($50^{+12}_{-12}\%$ versus $25^{+6}_{-5}\%$), though these differences are only significant at the $\sim2\sigma$ level. However, if we combine those AGNs classified as either "disturbed," which may represent the late phases of a major merger, and "interacting/merging and disturbed," we find that $75^{+8}_{-13}\%$ of the IR-only AGNs show signs of disturbance compared to only $31^{+6}_{-6}\%$ of the X-ray-only sample, a difference that is significant at the 3σ level. The vast majority of our admittedly small sample of IR-only AGNs therefore shows signs of clear merger activity and/or disturbances that may be indicative of recent mergers. This indicates that major mergers may indeed play a dominant role in fueling high-luminosity, heavily obscured AGN activity.

The morphologies and interaction classes of the AGNs that meet both the X-ray and IRAGN criteria tend to fall between those of the X-ray-only and IR-only samples. This implies that while Seyfert-luminosity AGNs are not predominantly associated with interacting and/or heavily disturbed hosts, the fraction of AGNs with disturbed morphologies may increase at higher luminosities/redshifts (i.e., the X-ray+IR sample) or as the nuclear obscuration increases (IRAGN-only). We examine

the independent impacts of luminosity and obscuration in Section 4.2.

Finally, it is worth noting that the increased merger fraction for our luminous, heavily obscured IR-only sample remains if we focus only on AGNs in the fixed redshift range of $z = 1.5 - 2.5$ where a majority of IR-only AGNs lie. Of the eight IR-only AGNs in this redshift range (six of which are selected both from the Sanders et al. 2007 and COSMOS15 catalogs), six (75%) are interacting or merging and disturbed. In contrast, only 2/12 X-ray+IR AGN (17%) are interacting (one is disturbed and the other is relatively undisturbed), and only 4/17 (24%) of the X-ray-only AGNs are interacting (three are disturbed and one is relatively undisturbed). In this redshift range, obscuration (e.g., X-ray detected or not) appears to play a larger role than luminosity (e.g., IRAGN or not), though these results may be biased by the small number of sources. Nevertheless, the significantly higher merger fraction among luminous and obscured IR-only AGNs in this limited redshift range suggests that the results for our full sample have not been highly biased by the larger average redshift of this sample compared to that of the X-ray selected AGN population.

4.2. Effects of Luminosity and Obscuration on Morphology

To determine if we can isolate the effects of luminosity and obscuration on the differences between the IR-only (high luminosity, heavily obscured) and X-ray only (lower luminosity, less obscured) populations, we plot in Figure 6 four of the the interaction classes as a function of both AGN bolometric luminosity (for luminosity bins with at least five AGNs) and obscuration. We also plot the sum of AGNs classified as either "interacting/merging and disturbed" or simply "disturbed." For

Table 1
Percentage of AGNs that Meet Morphology and Interaction Classes

Class	Sanders et al. (2007) IR-only AGN	Sanders et al. (2007) IR+X-ray (no BLAGN)	X-Ray-only AGN (no BLAGN)	COSMOS15 IR-only AGN	COSMOS15 IR+X-Ray no BLAGN	X-Ray-only AGN (restricted)[a] no BLAGN
Number of Sources	16	16	64	9	12	33
Disk	38^{+13}_{-10}	44^{+12}_{-11}	38^{+6}_{-6}	44^{+16}_{-14}	46^{+13}_{-12}	45^{+9}_{-8}
Spheroid	31^{+13}_{-9}	69^{+9}_{-13}	77^{+4}_{-6}	33^{+18}_{-11}	69^{+10}_{-15}	79^{+5}_{-9}
Irregular	50^{+12}_{-12}	12^{+13}_{-4}	9^{+5}_{-2}	56^{+14}_{-16}	8^{+14}_{-3}	18^{+9}_{-5}
Point Source	6^{+12}_{-2}	6^{+12}_{-2}	2^{+3}_{-0}	11^{+18}_{-4}	8^{+14}_{-3}	0^{+5}_{-1}
Asymmetric	69^{+9}_{-13}	25^{+13}_{-8}	17^{+6}_{-4}	56^{+14}_{-16}	23^{+15}_{-3}	21^{+9}_{-5}
Unclassifiable	0^{+10}_{-1}	0^{+10}_{-1}	$2^{+3}_{-0.0}$	0^{+17}_{-2}	0^{+12}_{-1}	0^{+5}_{-1}
Undisturbed	19^{+13}_{-6}	44^{+12}_{-11}	45^{+6}_{-6}	22^{+18}_{-8}	38^{+14}_{-11}	39^{+9}_{-8}
Undisturbed + Companion	0^{+10}_{-1}	6^{+12}_{-2}	8^{+5}_{-2}	0^{+17}_{-2}	8^{+14}_{-3}	9^{+8}_{-3}
Disturbed (D)	25^{+13}_{-8}	6^{+12}_{-2}	6^{+5}_{-2}	11^{+18}_{-4}	8^{+14}_{-3}	3^{+6}_{-1}
Interacting/Merging	56^{+11}_{-12}	44^{+12}_{-11}	39^{+6}_{-6}	67^{+11}_{-18}	46^{+13}_{-12}	48^{+9}_{-8}
Interacting/Merging, Undisturbed	6^{+12}_{-2}	0^{+10}_{-1}	14^{+5}_{-3}	11^{+18}_{-4}	0^{+12}_{-1}	21^{+9}_{-5}
Interacting/Merging and Disturbed (IMD)	50^{+12}_{-12}	44^{+12}_{-11}	25^{+6}_{-5}	56^{+14}_{-16}	46^{+13}_{-12}	27^{+9}_{-6}
IMD or D	75^{+8}_{-13}	50^{+12}_{-12}	31^{+6}_{-6}	67^{+11}_{-18}	54^{+12}_{-13}	30^{+9}_{-7}

Note.

[a] The X-ray AGNs in this column have been restricted to those sources that meet the Sanders et al. (2007) IRAC flux cuts and the COSMOS15 S/N cuts.

consistency with Figure 5, we exclude known BLAGNs (see also Section 4.1).

The fraction of AGNs classified as undisturbed appears to be independent of an AGN's bolometric luminosity, and while the fraction that are interacting/merging *and* disturbed (IMD) increases with luminosity, this drops again in the highest luminosity bin. This drop is offset in part by a rise in AGNs classified simply as disturbed (D) in the highest luminosity bin, such that the combination of "interacting/merging and disturbed" plus "disturbed" remains high at the highest luminosities. This trend is the opposite of those AGNs classified as "interacting/merging yet relatively undisturbed," which appear to be predominantly lower-luminosity Seyfert galaxies. However, luminosity and obscuration are not strictly independent in our sample: heavily obscured IR-only AGNs comprise a significant fraction of the two highest luminosity bins, and our sample does not contain lower-luminosity AGNs too obscured to be detected in the X-ray. It is therefore possible that the apparent increase in the disturbed fraction (IMD or D) at high luminosity is due at least in part to the heavily obscured IR-only AGNs in our sample. Indeed, the rise in IMD+D with luminosity is still present but not as pronounced if we consider only the X-ray selected AGNs.

Quantifying obscuration is somewhat more difficult than quantifying luminosity. Marchesi et al. (2016b) estimate X-ray column densities via X-ray spectral fitting for sources with >30 counts in the $0.5-7\,\mathrm{keV}$ band, but only 55% of our X-ray sources meet this criterion. For the remaining X-ray sources, we adopt the column density estimates from Marchesi et al. (2016a), which are based on the observed X-ray hardness ratios (or limits on the hardness ratios). If only an upper limit is available (9% of the X-ray sample), we take this to be consistent with no obscuration, and in cases where only a lower limit is available (13% of the X-ray sample), we adopt this lower limit as our measure of N_{H}. Furthermore, while we expect that the X-ray non-detected IRAGNs are heavily obscured, we do not know precisely how obscured they are.

Given these limitations, we plot in Figure 6(b) the samples with $N_{\mathrm{H}} < 10^{22}$, $10^{22} < N_{\mathrm{H}} < 10^{23}$, $10^{23} < N_{\mathrm{H}} < 10^{24}$, along with the IR-only AGNs.

While the undisturbed fraction is lowest for the heavily obscured IR-only AGNs, this trend is not statistically significant. Likewise, the "disturbed" and "interacting/merging and disturbed" fractions are highest for the IR-only population, but only marginally so, and while the sum of these disturbed categories (IMD+D) is highest for the IR-only AGNs, there is no clear trend with obscuration for the X-ray detected AGNs.

Disentangling the effects of luminosity and obscuration is therefore challenging, both due to our small sample size and the correlation between luminosity and obscuration, particularly for the IR-only subsample. It appears plausible that both luminosity and obscuration impact the morphology of our sample, but far more complete samples lacking a bias against low-luminosity, heavily obscured AGNs would be required to draw a definitive conclusion (see, for instance, Kocevski et al. 2015, who find that more heavily obscured AGNs show an increase in disturbed morphologies.)

4.3. Comparison to Previous Results

We plot in Figure 7 the consensus morphology classes of our sample as a function of redshift/X-ray luminosity and IRAC color, and overplot the redshift and luminosity regimes sampled by the studies of Cisternas et al. (2011b), Silverman et al. (2011), Kocevski et al. (2012), and Kocevski et al. (2015). We see good agreement when we compare our morphology assessments to these prior studies. Silverman et al. (2011) found that $18\% \pm 8\%$ of $0.25 < z < 1.05$ Seyferts are in kinematic pairs (early mergers). Of the 16 AGNs in our sample that meet their selection criteria, 7 (44%) are interacting. However, 2 of these are in late mergers and 1 is in a minor merger, for an early merger fraction of 4/16, or 25%, consistent with the Silverman et al. (2011) result.
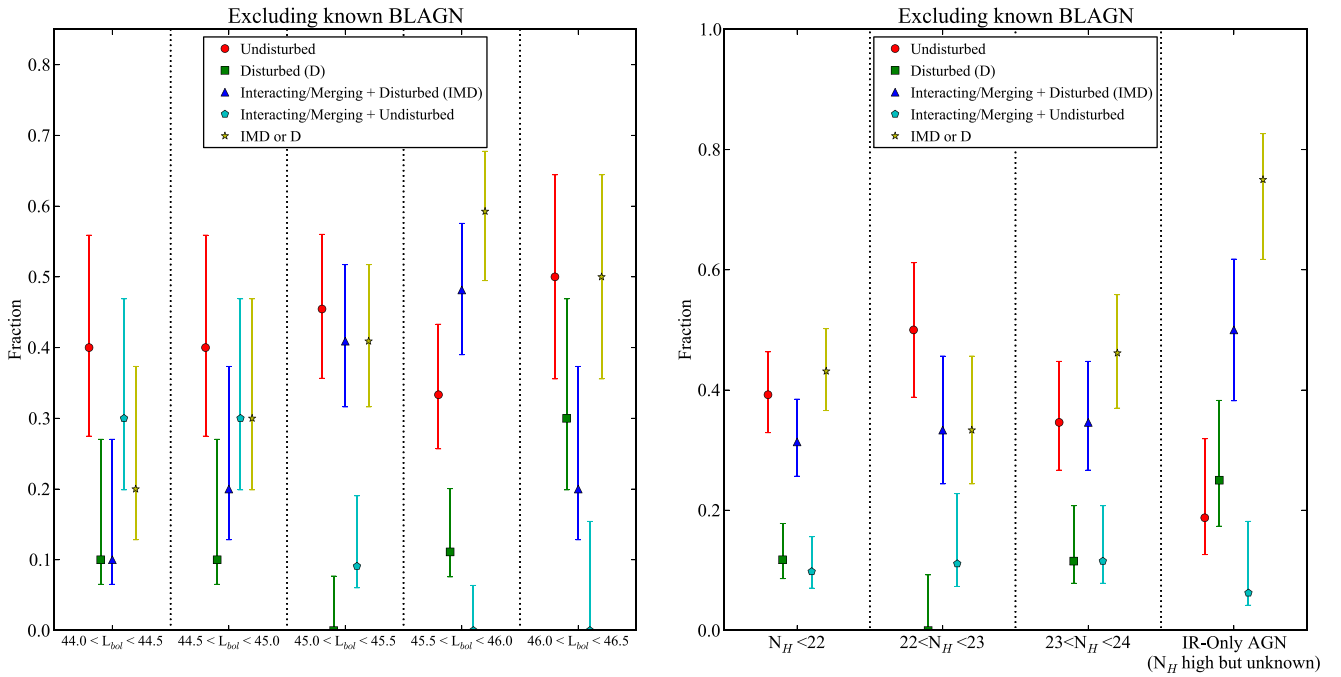
Figure 6. AGN interaction classes as a function of AGN bolometric luminosity in units of erg s^{-1} (left) and AGN obscuration in units of log cm^{-2} (right). As in Figure 5, we exclude known BLAGNs from the sample (see Section 4.1). While both luminosity and obscuration may impact the morphology of our sample, luminosity and obscuration are not strictly independent in our sample due to the inclusion of the IR-only AGNs (high luminosity/high obscuration AGNs). A larger and less biased sample is required to isolate the effects of luminosity and obscuration.

In a similar redshift regime that extends to both higher and lower luminosities, Cisternas et al. (2011b) found that 54% of AGNs were undisturbed, 31% were mildly distorted, and 15% were strongly distorted. Of the 17 sources in our sample that meet their selection criteria, 9 (53%) are undisturbed, 3 (18%) are interacting/merging yet relatively undisturbed, and 5 (29%) are interacting/merging and disturbed. However, 2 of these interacting/merging and disturbed AGNs are relatively minor disturbances that may have fallen in the "mildly distorted" bin. Generally, we are again in good agreement with this prior study.

A direct comparison to the Kocevski et al. (2015) study of $z < 1.5$ X-ray selected AGNs is difficult as their sample is split into subsamples with different X-ray obscurations, with each subsample covering a broad range of both luminosities and redshifts. If we focus only on their most obscured AGNs with $N_H > 23.5$ cm^{-2} and compare to our IR-only sample that falls within the same redshift bounds, we see a larger merger fraction (50%) than they report (22%). However, our heavily obscured IR-only AGNs are predominantly quasars, whereas a significant fraction of their highly obscured AGNs have Seyfert-like luminosities. The higher merger fraction observed in our work may therefore be due to the systematically higher luminosity of our sample (see Section 1 and the references therein).

Finally, Kocevski et al. (2012) looked at the CANDELS morphologies of higher-redshift X-ray AGNs. They find that 19% of $L_x > 10^{43}$ erg s^{-1} AGNs are interacting/merging and 47% are undisturbed. Of the 26 sources in our sample that meet their selection criteria, 5 (19%) are interacting/merging, and 16 (62%) are undisturbed. We therefore conclude that our findings for lower luminosity and/or lower redshift AGNs are consistent with findings in the literature that conclude that mergers do not play a dominant role in the fueling of Seyfert

galaxies at either low ($z < 1$) or high ($z \sim 2$) redshift, even if they may be responsible for driving AGN activity in higher luminosity, higher redshift, and more heavily obscured AGNs.

4.4. Undisturbed Disks

Constraining the role of major mergers in fueling AGN activity can be complicated by a potential time delay between the merger and the peak of AGN activity. However, as disks are expected to be disrupted or destroyed by major mergers, the undisturbed disk fraction can be used to place a constraint on the fraction of AGNs that are unlikely to have undergone a major merger, at least in the recent past. Of the X-ray-only AGNs, 16% are classified as undisturbed galaxies with a disk component, as are a similar fraction (4/27, or 15%) of X-ray +IR AGNs. Of the X-ray non-detected IRAGNs, however, only 1/16 (6%) is undisturbed with a disk component. The fraction of relatively undisturbed disks is therefore low across our sample. However, a non-negligible fraction of both X-ray-only and X-ray+IR AGNs lie in undisturbed disks, indicating that both moderate and high-luminosity AGN activity can occur in the absence of any recent major interaction. The undisturbed disk fraction is even lower, however, for the IR-only AGNs, suggesting that it may be less common for these AGNs to be triggered in isolation.

5. Conclusions

In summary, using the deep CANDELS NIR imaging in the CANDELS/COSMOS field, we have compared the rest-frame visual morphologies of X-ray and IR-selected AGNs. The X-ray-only AGNs in our sample cover a range of redshifts and tend to be Seyfert-luminosity AGNs with low to moderate obscuration. They are the least likely to be disturbed and the most likely to have a spheroidal component. When they are
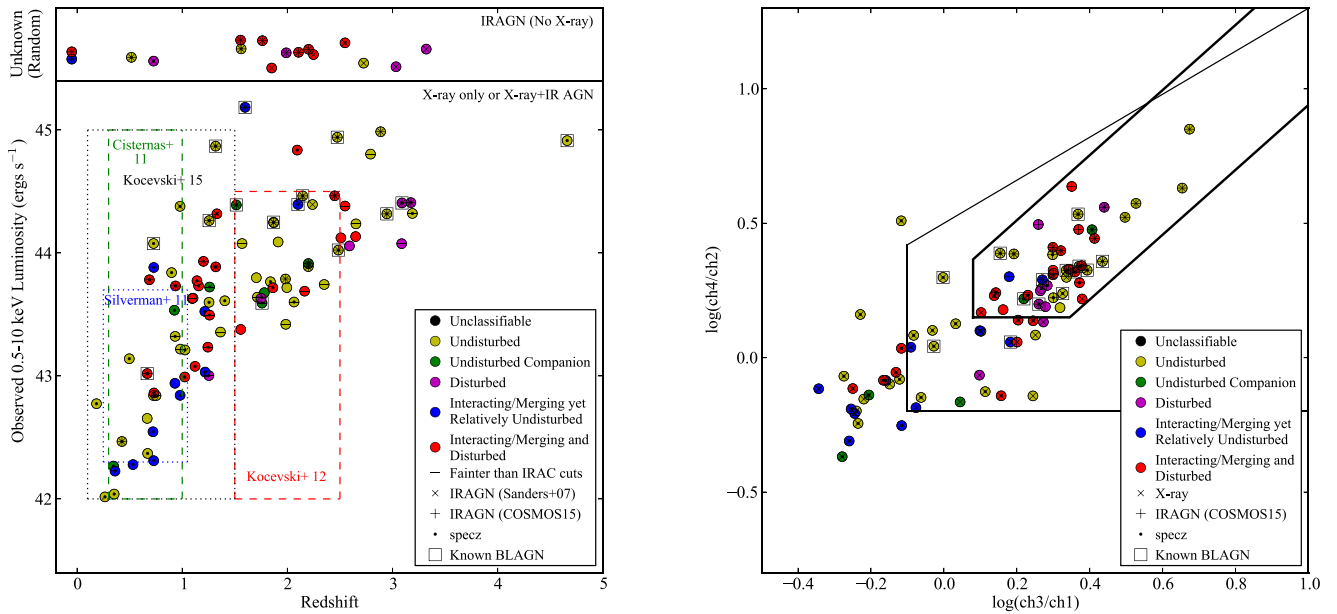
Figure 7. Consensus interaction class for our full sample as a function of both X-ray luminosity and redshift (left) and IRAC color (right). The regimes sampled by several previous studies are shown as dotted lines. In addition to interaction class, we indicate those AGNs that are X-ray or IR-detected, as well as those with spectroscopic redshifts and those known to be BLAGNs. The AGN selection region from Donley et al. (2012) is plotted on the IRAC color plot on the right, as is the larger AGN wedge of Lacy et al. (2007).

interacting or merging, the primary host galaxy often appears to remain relatively undisturbed, either because the merger is comparatively minor or because it is in an early phase more accurately described as a close pair. This suggests that low obscuration Seyfert-luminosity activity either precedes the high-luminosity, heavily dust enshrouded phase predicted during a major merger (for close pairs that will later become a major merger), that low level AGN activity can be triggered by minor interactions, or that this activity is unrelated to the nearby companion. Our findings for the X-ray sample are consistent with past studies that have concluded that mergers are not a dominant source of fueling at low AGN luminosity and obscuration (e.g., Cisternas et al. 2011b; Silverman et al. 2011; Kocevski et al. 2012).

While stochastic fueling may account for Seyfert-luminosity AGNs, models of galaxy and AGN formation suggests that major mergers are the dominant fueling mechanism for luminous, obscured AGNs and their hosts (e.g., Hopkins et al. 2008). The IR-only AGNs in our sample also span a range of redshifts, but unlike the X-ray-only sample, they tend to be high-luminosity, heavily obscured AGNs. These AGNs are significantly ($>3\sigma$) more likely than X-ray-only AGNs to have been classified as irregular or asymmetric and are also more likely than X-ray-only AGNs (at the $\sim2\sigma$ level) to be classified both as undergoing interactions/mergers that significantly disrupt the host galaxy and as simply "disturbed," which could potentially indicate the late stages of a merger. Combining these two categories, we find that 75% of IR-only AGNs show significant signs of disturbance compared to only 31% of the X-ray-only sample, a difference that is significant at the 3σ level. These results are consistent with theoretical models of galaxy and AGN growth as well as with recent observational evidence for an increase in the merger fraction at high luminosity and/or obscuration (Guyon et al. 2006; Kartaltepe et al. 2010; Koss et al. 2010, 2012; Treister et al. 2012; Urrutia et al. 2012; Satyapal et al. 2014; Kocevski

et al. 2015; Ellison et al. 2016; Fan et al. 2016; Shangguan et al. 2016; Weston et al. 2017).

The lack of evidence for merger-driven AGN growth in typical Seyfert-luminosity, X-ray selected AGNs (Sánchez et al. 2004; Grogin et al. 2005; Pierce et al. 2007; Gabor et al. 2009; Cisternas et al. 2011b; Schawinski et al. 2011; Kocevski et al. 2012; Simmons et al. 2012; Villforth et al. 2014; Rosario et al. 2015; Bruce et al. 2016) can therefore be attributed to looking for mergers among the wrong population of AGNs/hosts. By targeting luminous and heavily obscured AGNs using IR selection, we have selected exactly the sample of AGNs most likely to be merger driven, and indeed find evidence that the vast majority are heavily disturbed.

ORCID iDs

J. L. Donley ⓘ https://orcid.org/0000-0002-6589-2017
J. Kartaltepe ⓘ https://orcid.org/0000-0001-9187-3605
M. Salvato ⓘ https://orcid.org/0000-0001-7116-9303
P. Santini ⓘ https://orcid.org/0000-0002-9334-8705
H. Suh ⓘ https://orcid.org/0000-0002-2536-1633
A. M. Koekemoer ⓘ https://orcid.org/0000-0002-6610-2048
J. Trump ⓘ https://orcid.org/0000-0002-1410-0470

M. Brusa ⓘ https://orcid.org/0000-0002-5059-6848
C. Cardamone ⓘ https://orcid.org/0000-0003-4608-6340
A. Castro ⓘ https://orcid.org/0000-0002-7832-5337
M. Cisternas ⓘ https://orcid.org/0000-0002-3953-7839
C. Conselice ⓘ https://orcid.org/0000-0003-1949-7638
D. Croton ⓘ https://orcid.org/0000-0002-5009-512X
N. Hathi ⓘ https://orcid.org/0000-0001-6145-5090
C. Liu ⓘ https://orcid.org/0000-0002-4314-8713
R. A. Lucas ⓘ https://orcid.org/0000-0003-1581-7825
D. Rosario ⓘ https://orcid.org/0000-0002-0001-3587
D. Sanders ⓘ https://orcid.org/0000-0002-1233-9998
B. Simmons ⓘ https://orcid.org/0000-0001-5882-3323
C. Villforth ⓘ https://orcid.org/0000-0002-8956-6654
D. M. Alexander ⓘ https://orcid.org/0000-0002-5896-6313
E. F. Bell ⓘ https://orcid.org/0000-0002-5564-9873
N. A. Grogin ⓘ https://orcid.org/0000-0001-9440-8872
J. Lotz ⓘ https://orcid.org/0000-0003-3130-5643

References

Alexander, D. M., & Hickox, R. C. 2012, NewAR, 56, 93
Alonso-Herrero, A., Pérez-González, P. G., Alexander, D. M., et al. 2006, ApJ, 640, 167
Altamirano-Dévora, L., Miyaji, T., Aceves, H., et al. 2016, RMxAA, 52, 11
Bahcall, J. N., Kirhakos, S., Saxe, D. H., & Schneider, D. P. 1997, ApJ, 479, 642
Bennert, N., Canalizo, G., Jungwiert, B., et al. 2008, ApJ, 677, 846
Bruce, V. A., Dunlop, J. S., Mortlock, A., et al. 2016, MNRAS, 458, 2391
Brusa, M., Civano, F., Comastri, A., et al. 2010, ApJ, 716, 348
Cameron, E. 2011, PASA, 28, 128
Canalizo, G., & Stockton, A. 2001, ApJ, 555, 719
Cappelluti, N., Brusa, M., Hasinger, G., et al. 2009, A&A, 497, 635
Cattaneo, A., Combes, F., Colombi, S., Bertin, E., & Melchior, A.-L. 2005, MNRAS, 359, 1237
Cisternas, M., Jahnke, K., Bongiorno, A., et al. 2011a, ApJL, 741, L11
Cisternas, M., Jahnke, K., Inskip, K. J., et al. 2011b, ApJ, 726, 57
Civano, F., Elvis, M., Brusa, M., et al. 2012, ApJS, 201, 30
Civano, F., Marchesi, S., Comastri, A., et al. 2016, ApJ, 819, 62
Di Matteo, T., Springel, V., & Hernquist, L. 2005, Natur, 433, 604
Donley, J. L., Koekemoer, A. M., Brusa, M., et al. 2012, ApJ, 748, 142
Donley, J. L., Rieke, G. H., Alexander, D. M., Egami, E., & Pérez-González, P. G. 2010, ApJ, 719, 1393
Donley, J. L., Rieke, G. H., Pérez-González, P. G., & Barro, G. 2008, ApJ, 687, 111
Donley, J. L., Rieke, G. H., Pérez-González, P. G., Rigby, J. R., & Alonso-Herrero, A. 2007, ApJ, 660, 167
Dunlop, J. S., McLure, R. J., Kukula, M. J., et al. 2003, MNRAS, 340, 1095
Ellison, S. L., Patton, D. R., Mendel, J. T., & Scudder, J. M. 2011, MNRAS, 418, 2043
Ellison, S. L., Teimoorinia, H., Rosario, D. J., & Mendel, J. T. 2016, MNRAS, 458, L34
Engel, H., Tacconi, L. J., Davies, R. I., et al. 2010, ApJ, 724, 233
Fan, L., Han, Y., Fang, G., et al. 2016, ApJL, 822, L32
Gabor, J. M., Impey, C. D., Jahnke, K., et al. 2009, ApJ, 691, 705
Gebhardt, K., Bender, R., Bower, G., et al. 2000, ApJL, 539, L13

Glikman, E., Simmons, B., Mailly, M., et al. 2015, ApJ, 806, 218
Greene, J. E., Zakamska, N. L., Liu, X., Barth, A. J., & Ho, L. C. 2009, ApJ, 702, 441
Grogin, N. A., Conselice, C. J., Chatzichristou, E., et al. 2005, ApJL, 627, L97
Guyon, O., Sanders, D. B., & Stockton, A. 2006, ApJS, 166, 89
Hasinger, G. 2008, A&A, 490, 905
Hasinger, G., Cappelluti, N., Brunner, H., et al. 2007, ApJS, 172, 29
Hopkins, P. F., & Hernquist, L. 2006, ApJS, 166, 1
Hopkins, P. F., & Hernquist, L. 2009, ApJ, 698, 1550
Hopkins, P. F., Hernquist, L., Cox, T. J., et al. 2006, ApJS, 163, 1
Hopkins, P. F., Hernquist, L., Cox, T. J., & Kereš, D. 2008, ApJS, 175, 356
Hopkins, P. F., Kocevski, D. D., & Bundy, K. 2014, MNRAS, 445, 823
Hopkins, P. F., Richards, G. T., & Hernquist, L. 2007, ApJ, 654, 731
Ilbert, O., Capak, P., Salvato, M., et al. 2009, ApJ, 690, 1236
Ivison, R. J., Smail, I., Amblard, A., et al. 2012, MNRAS, 425, 1320
Kartaltepe, J. S., Mozena, M., Kocevski, D., et al. 2015, ApJS, 221, 11
Kartaltepe, J. S., Sanders, D. B., Le Floc'h, E., et al. 2010, ApJ, 721, 98
Kocevski, D. D., Brightman, M., Nandra, K., et al. 2015, ApJ, 814, 104
Kocevski, D. D., Faber, S. M., Mozena, M., et al. 2012, ApJ, 744, 148
Koekemoer, A. M., Faber, S. M., Ferguson, H. C., et al. 2011, ApJS, 197, 36
Koss, M., Mushotzky, R., Treister, E., et al. 2012, ApJL, 746, L22
Koss, M., Mushotzky, R., Veilleux, S., & Winter, L. 2010, ApJL, 716, L125
Lacy, M., Petric, A. O., Sajina, A., et al. 2007, AJ, 133, 186
Laigle, C., McCracken, H. J., Ilbert, O., et al. 2016, ApJS, 224, 24
Larson, K. L., Sanders, D. B., Barnes, J. E., et al. 2016, ApJ, 825, 128
Magorrian, J., Tremaine, S., Richstone, D., et al. 1998, AJ, 115, 2285
Marchesi, S., Civano, F., Elvis, M., et al. 2016a, ApJ, 817, 34
Marchesi, S., Lanzuisi, G., Civano, F., et al. 2016b, ApJ, 830, 100
Mechtley, M., Jahnke, K., Windhorst, R. A., et al. 2016, ApJ, 830, 156
Nayyeri, H., Hemmati, S., Mobasher, B., et al. 2017, ApJS, 228, 7
Pierce, C. M., Lotz, J. M., Laird, E. S., et al. 2007, ApJL, 660, L19
Reichard, T. A., Heckman, T. M., Rudnick, G., et al. 2009, ApJ, 691, 1005
Robertson, B., Hernquist, L., Cox, T. J., et al. 2006, ApJ, 641, 90
Rosario, D. J., McIntosh, D. H., van der Wel, A., et al. 2015, A&A, 573, A85
Salvato, M., Ilbert, O., Hasinger, G., et al. 2011, ApJ, 742, 61
Sánchez, S. F., Jahnke, K., Wisotzki, L., et al. 2004, ApJ, 614, 586
Sanders, D. B., Salvato, M., Aussel, H., et al. 2007, ApJS, 172, 86
Sanders, D. B., Soifer, B. T., Elias, J. H., et al. 1988, ApJ, 325, 74
Santini, P., Rosario, D. J., Shao, L., et al. 2012, A&A, 540, A109
Satyapal, S., Ellison, S. L., McAlpine, W., et al. 2014, MNRAS, 441, 1297
Schawinski, K., Simmons, B. D., Urry, C. M., Treister, E., & Glikman, E. 2012, MNRAS, 425, L61
Schawinski, K., Treister, E., Urry, C. M., et al. 2011, ApJL, 727, L31
Shangguan, J., Liu, X., Ho, L. C., et al. 2016, ApJ, 823, 50
Silverman, J. D., Kampczyk, P., Jahnke, K., et al. 2011, ApJ, 743, 2
Simmons, B. D., Urry, C. M., Schawinski, K., Cardamone, C., & Glikman, E. 2012, ApJ, 761, 75
Suh, H., Civano, F., Hasinger, G., et al. 2017, ApJ, 841, 102
Treister, E., Schawinski, K., Urry, C. M., & Simmons, B. D. 2012, ApJL, 758, L39
Urrutia, T., Lacy, M., & Becker, R. H. 2008, ApJ, 674, 80
Urrutia, T., Lacy, M., Spoon, H., et al. 2012, ApJ, 757, 125
Veilleux, S., Kim, D.-C., Rupke, D. S. N., et al. 2009a, ApJ, 701, 587
Veilleux, S., Rupke, D. S. N., Kim, D., et al. 2009b, ApJS, 182, 628
Villforth, C., Hamann, F., Rosario, D. J., et al. 2014, MNRAS, 439, 3342
Villforth, C., Hamilton, T., Pawlik, M. M., et al. 2017, MNRAS, 466, 812
Weston, M. E., McIntosh, D. H., Brodwin, M., et al. 2017, MNRAS, 464, 3882
Zakamska, N. L., Strauss, M. A., Krolik, J. H., et al. 2006, AJ, 132, 1496